JOURNAL OF GEOPHYSICAL RESEARCH, VOL. ???, XXXX, DOI:10.1029/,

A topside equatorial ionospheric density and composition climatology during and after extreme solar minimum

J. H. Klenzing,[1] F. Simões,[1] S. Ivanov,[2] R. A. Heelis,[3] D. Bilitza,[4,5] R. F. Pfaff,[1] and D. E. Rowland[1]

J. H. Klenzing, Space Weather Lab / Code 674, Goddard Space Flight Center, Greenbelt, Maryland, USA (jeffrey.klenzing@nasa.gov)

[1] Space Weather Lab / Code 674, Goddard Space Flight Center, Greenbelt, Maryland, USA

[2] Department of Physics, Georgia Institute of Technology, Atlanta, Georgia, USA

[3] Center for Space Sciences, University of Texas at Dallas, Richardson, Texas, USA

[4] Heliophysics Laboratory / Code 672, Goddard Space Flight Center, Greenbelt, Maryland, USA

[5] Department of Physics, George Mason University, Fairfax, Virginia, USA

Abstract. During the recent solar minimum, solar activity reached the lowest levels observed during the space age. This extremely low solar activity has accompanied a number of unexpected observations in the Earth's ionosphere and thermosphere when compared to previous solar minima. Among these are the fact that the ionosphere is significantly contracted beyond expectations based on empirical models. Climatological altitude profiles of ion density and composition measurements near the magnetic dip equator are constructed from the C/NOFS satellite to characterize the shape of the topside ionosphere during the recent solar minimum and into the new solar cycle. The variation of the profiles with respect to local time, season, and solar activity are compared to the IRI-2007 model. Building on initial results reported by *Heelis et al.* [2009], here we describe the extent of the contracted ionosphere, which is found to persist throughout 2009. The shape of the ionosphere during 2010 is found to be consistent with observations from previous solar minima.

1. Introduction

The solar minimum between cycles 23 and 24 has been an unusual period of solar activity. The minimum was expected to occur in 2006, but instead solar activity continually decreased throughout 2007 and 2008 [*Russell et al.*, 2010]. Traditional proxies for solar activity such F10.7 (the flux of solar radiation at 10.7 cm wavelength) have "bottomed out," while actual measurements of the EUV flux have continued to decrease [*Araujo-Pradere et al.*, 2011; *Chen et al.*, 2011]. Some long-term climate modelers have even speculated that the deepest part of this minimum could be used to better understand the Maunder minimum [*Schrijver et al.*, 2011].

A number of surprising observations in the ionosphere and thermosphere has accompanied this period of extremely low solar activity. The thermospheric density was found to reach record lows based on the analysis of the orbital decay of numerous satellites [*Emmert et al.*, 2010] and by *in situ* measurement of the neutral scale-height [*Haaser et al.*, 2010]. *Solomon et al.* [2011] showed that this reduction in thermospheric density was largely due to low solar activity and that other secular variations (such as geomagnetic activity) were small in comparison.

Heelis et al. [2009] showed that the ionosphere was contracted as well, with the transition height between H^+ and O^+ being significantly lower than predicted by the IRI model. Additionally, the topside nighttime ion temperatures have been found to be relatively cold compared to IRI at an altitude of 400 km, as low as 600 K [*Coley et al.*, 2010]. The average ion drift in the topside ionosphere has been found to be significantly different from previous observations, including other solar minima. The $\mathbf{E}\times\mathbf{B}$ drift climatology observed by the C/NOFS satellite was found to differ from the Fejer-Scherliess model [*e.g.*, *Scherliess and Fejer*, 1999], including downward afternoon drifts in some regions as well as a weak to non-existent pre-reversal enhancement [*Pfaff et al.*, 2010].

The behavior of the topside ionosphere during solar minimum has been well-documented through *in situ* measurements [*Greenspan et al.*, 1994; *West et al.*, 1997], topside sounders [*Benson and Bilitza*, 2009], and ground-based radar [*Hysell et al.*, 2009]. However, because solar activity is lower during the cycle 23/24 minimum than during the last few solar cycles, current empirical models must extrapolate based on previous observations. Long-term monitoring of ionospheric density by the CHAMP and GRACE satellites reveal that the IRI-2007 model overestimates the expected density leading up to and including the recent solar minimum [*Lühr and Xiong*, 2010].

In this study, the ion density and composition data from the C/NOFS satellite are used to construct climatological maps of density and composition as a function of altitude and local time near the magnetic dip equator. The maps are divided into season and solar activity in order to understand the shape of the topside ionosphere during this extreme solar minimum, as well as its evolution on the journey back to solar maximum. These climatology maps are compared to the results from the IRI-2007 model. The highly contracted ionosphere is found to persist throughout 2009, well into the new solar cycle.

2. Measurements and Models

The Communication/Navigation Outage Forecast System (C/NOFS) satellite is part of a space weather mission led by the US Air Force Research Laboratory to locate, understand, and predict equatorial ionospheric scintillation [*de La Beaujardière et al.*, 2004]. The C/NOFS satellite was launched in April 2008 into a 13° inclination orbit with perigee near 400 km and apogee near 860 km. This elliptical orbit allows for a sampling of ion density over multiple scale heights of the topside ionosphere. The C/NOFS perigee precesses through all solar local times roughly once every 65 days. C/NOFS is equipped with multiple instrument suites designed to study the ion and neutral populations and their effect on the propagation of communication signals.

This study will focus on the total ion density (electron density for a quasi-neutral plasma) and the H^+ and O^+ components. The total density and composition are obtained from a Retarding Potential Analyzer (RPA), part of the Coupled Ion-Neutral Dynamics Investigation (CINDI) suite of instruments on board C/NOFS. The well-established RPA technique consists of using a series of biased grids to select certain energies of ions to measure as a current [*Heelis and Hanson*, 1998]. By sweeping over a range of voltages, the relative contribution of each ion species (along with ion drift velocity and temperature) can be calculated.

The International Reference Ionosphere (IRI) is considered the international standard model for calculating empirically-derived ionospheric parameters based on both ground-based and satellite measurements [*Bilitza and Reinisch*, 2008]. IRI was founded as a joint project between the Committee on Space Research (COSPAR) and by the International Union of Radio Science (URSI). An empirical model was chosen for comparison to the C/NOFS observations in order to better illustrate the differences between the topside density variations when compared to previous solar minima. The IRI model can generate estimated values of density and ion composition for a given input of solar activity, which is described by the geophysical indices Rz (based on the sunspot number) and IG (based on the ionospheric response) [*Bilitza*, 2000].

The international sunspot number (Rz, also referred to as Ri after the main observation platform moved from Zürich to Brussels in 1980) is a weighted average of the number of sunspots observed on the surface of the sun [*Clette et al.*, 2007]. The weighting is designed to account for the differences between individual sunspots and clusters of sunspots. The IG index was developed by *Liu et al.* [1983] to provide an estimate of the peak F2-region density based on the International Radio Consultative Committee (CCIR) maps of the ionosphere. To do this, the index uses a weighted average of ionosonde measurements around the world similar to the method introduced by *Minnis and Bazzard* [1960]. This index is scaled to produce a "global effective sunspot number." However, since this calculation is based on the actual measurements of the ionosphere, it does not have a lower limit (unlike Rz, which by definition cannot be less than zero). During the prolonged solar minimum between cycles 23 and 24, IG is often negative. The IG index is provided by the UK World Data Center and is available in either monthly averages (IG) or 12-month averages (IG_{12}).

The NeQuick topside model is used to generate expected values of ion density and composition every five seconds along the orbit track of C/NOFS for every orbit through the end of 2010. The NeQuick model was chosen due to its excellent performance when compared to topside sounder measurements from the Alouette and ISIS missions relative to the other topside options included in IRI [*Bilitza et al.*, 2006; *Bilitza*, 2009]. For this study, the 12-month running averages of Rz (referred to as Rz_{12}) and IG (IG_{12}) are used. Only dates with the definitive values of Rz_{12} and IG_{12} (through January 2011 at the time of this writing) were used.

To illustrate the prolonged nature of the recent solar minimum, these activity proxies are compared for the last three solar cycles in Figure 1. Panel (a) shows the values of F10.7A (the 81-day average of F10.7) for 36 months around the minima between cycles 20 and 21 (1975, plotted in blue), cycles 21 and 22 (1986, plotted in green), cycles 22 and 23 (1996, plotted in orange), and cycles 23 and 24 (2008, plotted in red). The values of Rz_{12} and IG_{12} for the same three periods are plotted in panels (b) and (c), respectively. All three indices show that solar activity is deeper and longer than in previous years.

A sample portion of the data used in this study ($\sim$3 consecutive orbits) is shown in Figure 2. The CINDI measurements are shown as solid lines, the predicted IRI-2007 values are shown as dashed lines. Two examples are given to illustrate the effect of precession on the density variations: the 17 Nov event (a) shows three consecutive orbits during a period when perigee is near local noon; the 19 Dec event (b) shows a similar section of data when perigee is near local midnight. Note that the CINDI measurements are more variable than the IRI predictions.

3. Technique for Reconstructing Topside Profiles

The density measurements from C/NOFS are averaged together to create climatological altitude profiles. Because the elliptical orbit precesses through a variety of longitudes, the reconstructed profiles cannot be thought of as the ionospheric profile at any given location. Rather, these are average profiles that neglect longitudinal variations, tidal effects and local magnetic anomalies. (Such effects are small relative to the altitude and local time effects and will be the topic of a future study.) In order to be certain that any comparisons between the data and model are on equal footing, the algorithms used to reconstruct average topside profiles from the CINDI data are also used on the expected density values generated by IRI along each orbit of C/NOFS as shown in Figure 2.

The C/NOFS satellite undergoes a complete precession of perigee through all local times roughly once every 65 days. In order to better smooth out the variations due to the daily longitudinal precession, a period of 91 days is used for the reconstructed topside data. Data that is noisy or contains localized features such as plasma density depletions or enhancements are removed from the averages in order to approximate a true background density. To accomplish this, a Savitsky-Golay filter [*Savitsky and Golay*, 1964] is used on the C/NOFS data to determine the smoothness of the dataset. The smoothing window is 241 points wide (containing roughly two minutes of data), and the smoothing function is a third-degree polynomial. Because the filtered values represent an average of the perturbed and background densities, filtered values that differ by more than 0.5% from the measured value are removed from the averages.

The profiles are calculated every 0.5 hours in local time with a 10 km resolution. To smooth out the data, there is a significant overlap between each bin. (The bins are 2.5 hours wide and 50 km high.) Only points within ±2.5 deg magnetic dip latitude are used in the reconstruction, but all longitudes are used in the averages. To remove the effects of magnetic substorms, only quiet times where $\mathrm{Kp} \leq 3$ are used.

Figure 3a shows a sample dayside profile for the December Solstice of 2008 as reconstructed from CINDI data (shown in black) and from the IRI predictions (shown in green). The dashed lines represent the first and third quartiles for each bin. Part of this variaiton in the data set is due to the longitudinal variations. A sample post-sunset profile is shown in Figure 3b. Note that there is a sharp in the vertical gradient for the measured profile, while the IRI prediction varies smoothly. A similar effect was observed for higher magnetic latitudes in *Sibanda and McKinnell* [2011].

Figure 4 shows the average composition associated with the profiles in Figure 3. The solid lines represent the measured components of H^+ (red) and O^+ (blue), and the dashed lines represent the IRI expectations. Note that for both the dayside and nightside profiles, the measured concentration of O^+ is consistently lower than the expected value. This is consistent with previous findings that the ionosphere is contracted more than expected in the recent solar minima [*Heelis et al.*, 2009; *Lühr and Xiong*, 2010]. However, the H^+ component may be either larger or smaller than expected; it is consistently larger on the dayside profile in the altitude range of the C/NOFS satellite.

The transition height between O^+ and H^+ can be inferred from the figure by noting where the red curve crosses the blue curve for a given profile. The transition height for the CINDI profile in Figure 4b is is ∼50 km lower than the expected value based on IRI. This is consistent with the findings by *Heelis et al.* [2009] that the transition height is lower than expected during the recent solar minimum.

Figure 5 shows the composition profiles for the December solstice of 2010, two years after the deepest part of the recent solar minimum. The estimates of both components match the IRI predictions much better for the dayside profiles (5a), as well as the O^+ component for the post-sunset profile (5b). The H^+ component is low by a factor of 4 for the upper altitudes.

Density and composition profiles as shown in Figures 3-4 are generated for every 0.5 hours of local time for 91-day seasons ranging from the December solstice of 2008 to the December solstice of 2010. The variations of the topside density profiles with respect to local time and season are discussed in the following two sections. The seasonal divisions and the associated average solar indices are listed in Table 1. (The final season is cut short by 4 days due to the current availability of definitive values for the Rz_{12} and IG_{12} indices for driving the IRI model). The two equinoctial seasons remain separate in order to better capture the effects of the slowly increasing solar activity.

4. Variation with Local Time

Figure 6 is the summary plot for the December Solstice of 2008. (This corresponds to the deepest part of the cycle 23/24 minimum.) Panel (a) shows the average total density as measured by CINDI as a function of altitude and solar local time, and panel (b) shows the equivalent average from the IRI-2007 values generated over the C/NOFS orbits. The transition height between H^+ and O^+ as calculated from the average reconstructed profiles is plotted over the contour maps as a solid (CINDI) or a dashed (IRI) black line. Figure 6c is the ratio of the IRI average density to that computed from CINDI. (Both the measured and modeled transition heights are included in this panel for reference.) Similarly reconstructed profiles for the concentrations of O^+ and H^+ are shown in Figures 6d-i.

Note that over the full range of altitudes and local times covered by the C/NOFS satellite, there can be found regions where the IRI-2007 model will either overestimate or underestimate density, whether it be total density (panel c), O^+ concentration (f), or H^+ concentration (i). *Lühr and Xiong* [2010] found that IRI tended to overestimate total density during solar min; this study was conducted with the CHAMP and GRACE satellites, which are in circular orbits at 310 and 490 km altitude, respectively. Similarly, for a fixed local altitude near the C/NOFS perigee, Figure 6c shows that the IRI model overestimates total density for all local times except near the dawnside terminator. Averaging over all local times at 490 km, IRI overestimates the C/NOFS density by about 80% for this time period, which is consistent with the GRACE results.

Several additional features of the contracted ionosphere are clearly seen in Figure 6. In particular, the post-sunset electron density is lower than predicted by up to a factor of 4 (6c), and the concentration of O^+ is generally smaller than predicted for all local times (6f), except near the dawnside terminator. The measured concentration of H^+ is larger than estimated by IRI on the dayside profiles and for the nightside below the transition height.

Figures 7 and 8 show similar density maps for the December solstices of 2009 and 2010, respectively. It is readily apparent that the densities for the March equinox of 2010 are much closer to the expected values. For instance, both the ratio plots for total density (c) and O^+ concentration (e) are significantly closer to one when compared to the previous year. However, there are still some discrepancies between model and data, such as near sunrise and above the transition height post sunset. The estimates of H^+ for 2010 are high on the nightside and low on the dayside.

5. Variation with Season and Solar Activity

Climatological maps similar to those shown in Figures 6-8 were generated for each season shown in Table 1. In order to better illustrate the effects of seasons and solar activity, certain metrics will be adopted. Figure 9 shows the vertical “total electron content” (TEC) between 400 and 800 km. (This should not be confused with the total electron content in the typical sense, since we only observe over a relatively small range of altitudes above the F2-peak. However, it is instructive to display the relative changes in this metric.) Because the height of apogee drops over the lifetime of the satellite (822 km as of 31 January 2011), 800 km was chosen as the upper limit for the integrated density measurements for the purposes of this metric (although the total density above 800 km is minimal). The integrated vertical density is plotted in TEC units (TECU), or units of 10^{16} m^{-3}. Each panel represents a given season and contains the $TEC_{400-800}$ calculated from the CINDI measurements for each available year plotted as solid lines, with data from 2008 plotted in green, 2009 in purple, and 2010 in orange. The corresponding $TEC_{400-800}$ as calculated from IRI-2007 is shown in dashed lines.

The measured densities are significantly lower for all local times through the December solstice of 2009. For the March equinox of 2010 (the orange line in Figure 9c), the integrated density is ∼25% larger than the model on the dayside. For the two following seasons in 2010, the modeled values better approximate the CINDI measurements than in the previous seasons. Additionally, the CINDI measurements in the December solstice of 2009 are still very close to those from 2008, while there is a dramatic increase in density for the March equinox of 2010. This corresponds to a rise in F10.7 above 80 sfu. Additionally, the average effective sunspot number (IG_{12}) based on the ionospheric activity more closely matches the measured sunspot number (Rz_{12}) for this period.

Another interesting feature is that the measured ion density in March equinox of 2010 is larger than the corresponding density in the September equinox of the same year. The TEC plots from these two periods have been replotted in a single panel in Figure 10 to better illustrate this asymmetry. All three of the solar/ionospheric activity proxies are larger in for the September equinox than the March period (see Table 1). Accordingly, the IRI-2007 modeled values predict that the densities in September would be larger (the dashed orange lines) than those from March (dashed purple lines). This is clearly not the case in the measured densities (represented by the solid lines). This equinoctial asymmetry is similar to that noted in the COSMIC TEC data by *Liu et al.* [2010]. A similar effect was recently reported in the vertical drift data from the ROCSAT-1 satellite [*Ren et al.*, 2011]. However, we should remember that the ROCSAT data is from a period when the solar activity was much higher, and an investigation into this equinoctial asymmetry utilizing the C/NOFS vertical drift data will be required to fully understand this ion density asymmetry.

The transition height between H^+ and O^+ is calculated from the reconstructed profiles for both data and model. These are shown with respect to seasonal and temporal variations in Figure 11 (similar to the integrated densities presented previously). Note that there is no significant difference between the nightside transition height as predicted by IRI over the course of the mission (the dayside transition heights are typically outside of the range of the C/NOFS satellite). The dayside transition heights for 2010 are still lower than predicted by the models, but it should be noted that these are consistent with observations from Atmospheric Explorer from a previous solar minimum [*González et al.*, 1992]. The nightside transition heights for 2010 are consistent with that predicted by IRI.

6. Discussion

The reduced densities observed during the extreme portion of the recent solar minimum could be explained by any combination of the following effects:

1. The height of the F2 layer (hmF2) is lower than predicted.
2. The density of the F2 peak (NmF2) is lower than predicted.

3. The shape of the topside ionosphere is different.

Because the peak of the F layer is below the C/NOFS perigee (400 km) for most of the mission, we cannot comment on the cause from this data alone. (C/NOFS travelled below the F peak for the first time in April 2011.) Figure 12 is provided to illustrate this problem. An initial ion density profile is generated from IRI-2007 (shown in black) for the December solstice of 2008 for 1400 local time. Two modified profiles are created that would lead to the observed ∼67% overestimate in $\mathrm{TEC}_{400-800}$ shown in Figure 9. The first is created by simply scaling the density by a factor of 0.6 (shown in blue), the second is created by moving the F peak down by 65 km (shown in red).

While recent studies using ionosonde data have shown that NmF2 reached record low measurements during the recent solar minimum [*Liu et al.*, 2011], IRI-2007 is found to predict this density very well, with the standard deviations being comparable to previous solar cycles [*Bilitza et al.*, 2011]. This is due to the fact that the IRI model predicts the peak density based on the IG12 index, which is in itself a global average of ionosonde measurements.

The topside ionospheric density is controlled not just by solar radiation, but by a balance of chemical and dynamic processes. In the topside ionosphere, the creation of H^+ ions is primarily due to charge exchange with O^+ [*Rishbeth and Garriott*, 1969].

$$O^+ + H \rightleftharpoons O + H^+ \tag{1}$$

To first order approximation, the relation between the the ion components will then depend on the densities of the neutral components.

$$[H^+] = \frac{9}{8}\frac{[H]}{[O]}[O^+] \qquad (2)$$

The factor of 9/8 is due to statistical differences in the forward and reverse reaction rates. The increased concentration of H^+ in the topside ionosphere is consistent with the increased ratio of neutral $[H]/[O]$ observed in the upper thermosphere [*Haaser et al.*, 2010]. A recent study by *Hysell et al.* [2009] compared topside profiles from the Jicamarca Radar Observatory with the SAMI2 model and concluded that the shape of the H^+ fraction is also affected by the $\mathbf{E}\times\mathbf{B}$ drift time history as well.

This decreased post-sunset density may be partially related to the altered vertical drift climatology during the recent solar min. Unlike the Fejer-Schierless model, the vertical drift is found to be downward in the afternoon, and the large upward drift around sunset known as the pre-reversal enhancement is largely absent in the 2008 and 2009 data [*Pfaff et al.*, 2010]. The density structure may also be due to different climatologies in the meridional winds.

7. Summary and Conclusions

A statistical study of the ion density and composition in the topside ionosphere near the magnetic dip equator during the recent solar minimum was conducted. The major findings are the following:

1. While the overall ionosphere was found to be contracted relative to empirical expectations, the ratio of the expected density to the measured density was found to be a strong function of altitude and local time, including some areas (such as ∼800 km just

before dawn) where the average measured ion density was higher than predicted by as much as a factor of four.

2. During this contracted phase, $[H^+]$ is found to be greater than predicted by IRI-2007 for all observed altitudes (400 to 850 km) on the dayside and below the transition height for the nightside.

3. The shape of the topside nighttime ionosphere between 400 and 850 km was found to be different from the predicted shape. The profile generated by IRI varies smoothly, while the data shows a sharp change in the vertical gradient associated with the lower transition height.

4. The post-sunset ion density decreased more rapidly than expected based on previous solar minima. This may be related to a different drift climatology observed with the C/NOFS satellite during extreme solar min as previously reported by *Pfaff et al.* [2010].

5. This highly contracted ionosphere persisted until the March equinox of 2010, over a year into the new solar cycle. The transition heights observed in 2010 are are consistent with observations from previous solar minima.

6. The geophysical indices used to drive the IRI model, Rz_{12} and IG_{12}, are both significantly lower than in previous solar minima. The previously reported tendency of IRI to overestimate density during the extreme solar min is not a deficiency of the chosen input indices, but rather illustrates the fact that we have not observed the ionosphere during such a low period of solar activity. The reconstructed topside profiles from C/NOFS can be used as an additional constraint on future versions of IRI.

The C/NOFS satellite provides a unique look at the shape of the topside ionosphere. The topside data from C/NOFS during this unprecedented low in solar activity could be used as a constraint on future empirical models. Future studies will include regional case studies for comparison with ground-based measurements, as well as variations with longitude and magnetic latitude. Additionally, the reconstructed profiles can be used to discuss transport phenomena in the topside ionosphere in conjunction with drift climatologies using physics-based models to quantify the relative effects of altered transport and chemistry during extreme solar minimum.

Acknowledgments. JK and FS are supported by an appointment to the NASA Postdoctoral Program at Goddard Space Flight Center, administered by Oak Ridge Associated Universities through a contract with NASA. The work performed by SI was supported by the NASA Undergraduate Student Research Program. The work at the University of Texas at Dallas is supported by NASA grant NAS5-01068. The Communication/Navigation Outage Forecast System (C/NOFS) mission, conceived and developed by the Air Force Research Laboratory, is sponsored and executed by the USAF Space Test Program. F10.7, Rz_{12}, and IG_{12} are provided by the UK World Data Center.

References

Araujo-Pradere, E. A., R. Redmon, M. Fedrizzi, R. Viereck, T. J. Fuller-Rowell (2011), Some Characteristics of the Ionospheric Behavior During the Solar Cycle 23 24 Minimum, *Solar Phys.*, DOI 10.1007/s11207-011-9728-3.

Benson, R. F., and D. Bilitza (2009), New satellite mission with old data: Rescuing a unique data set, *Radio Sci., 44*, RS0A04, doi:10.1029/2008RS004036.

Bilitza, D. (2000), The importance of EUV indices for the international reference ionosphere, *Phys. Chem. Earth (C), 25*, pp. 515-52.

Bilitza, D., B. W. Reinisch, S. M. Radicella, S. Pulinets, T. Gulyaeva, and L Triskova (2006), Improvements of the International Reference Ionosphere model for the topside electron density profile, *Radio Sci., 41*, RS5S15, doi:10.1029/2005RS003370.

Bilitza, D., and B. W. Reinisch (2008), International Reference Ionosphere 2007: Improvements and new parameters, *Adv. Space Res., 43,* 599, doi:10.1016/j.asr.2007.07.048.

Bilitza, D. (2009), Evaluation of the IRI-2007 model options for the topside electron density, *Adv. Space Res., 44,* 701, doi:10.1016/j.asr.2009.04.036.

Bilitza, D., S. A. Browna, M. Y. Wang, and P. A. Roddy (2011), Measurements and IRI Model Predictions during the Recent Solar Minimum, *presented at URSI GASS 2011*, Session G02.4.

Chen, Y., L. Liu, and W. Wan (2011), Does the $F_{10.7}$ index correctly describe the solar EUV flux during the deep solar minimum of 2007-2009?, *J. Geophys. Res., 116*, A04304, doi:10.1029/2010JA016301.

Clette, F., D. Berghmans, P. Vanlommel, R. A. M. Van der Linden, A. Koeckelenbergh, and L. Wauters (2007), From the Wolf number to the International Sunspot Index: 25 years of SIDC, *Adv. Space Res., 40*, p 919928, doi:10.1016/j.asr.2006.12.045.

Coley, W. R., R. A. Heelis, M. R. Hairston, G. D. Earle, M. D. Perdue, R. A. Power, L. L. Harmon, B. J. Holt, and C. R. Lippincott (2010), Ion temperature and density relationships measured by CINDI from the C/NOFS spacecraft during solar minimum, *J. Geophys. Res., 115*, A02313, doi:10.1029/2009JA014665.

de La Beaujardière, O., and the C/NOFS Definition Team (2004), C/NOFS: a mission to forecast scintillations, *J. Atmos. and Sol-Terr. Phys,, 66,* 1573, doi:10.1016/j.jastp.2004.07.030.

Emmert, J. T., J. L. Lean, and J. M. Picone (2010), Record-low thermospheric density during the 2008 solar minimum, *Geophys. Res. Lett., 37,* L12102, doi:10.1029/2010GL043671.

González, S. A., B. G. Fejer, R. A. Heelis, and W. B. Hanson (1992), Ion Composition of theTopside Equatorial Ionosphere During Solar Minimum, *J. Geophys. Res., 97*, pp 4299-4303.

Greenspan, M. E., W. J. Burke, F. J. Rich, W. J. Hughes, and R. A. Heelis, DMSP F8 observations of the mid-latitude and low-latitude topside ionosphere near solar minimum, *J. Geophys. Res., 99*, pp 3817-3826.

Haaser, R. A., G. D. Earle, R. A. Heelis, W. R. Coley, and J. H. Klenzing (2010), Low-latitude measurements of neutral thermospheric helium dominance near 400 km during extreme solar minimum, *J. Geophys. Res., 115*, A11318, doi:10.1029/2010JA015325.

Heelis, R. A., and W. B. Hanson (1998), "Measurements of thermal ion drift velocity and temperature using planar sensors," in *Measurement Techniques in Space Plasmas (Geophys. Monogr. Ser. vol. 102)*, edited by R. F. Pfaff, J. E. Borovsky, and D. T. Young, (AGU, Washington, D. C., 1998) p. 61.

Heelis, R. A., W. R. Coley, A. G. Burrell, M. R. Hairston, G. D. Earle, M. D. Perdue, R. A. Power, L. L. Harmon, B. J. Holt, and C. R. Lippincott (2009), Behavior of the O+/H+ transition height during the extreme solar minimum of 2008, *Geophys. Res. Lett., 36,* L00C03, doi:10.1029/2009GL038652.

Hysell, D. L., J. L. Chau, and J. D. Huba (2009), Topside measurements at Jicamarca during solar minimum, *Ann. Geophys., 27*, pp 427439, www.ann-geophys.net/27/427/2009/.

Liu, R. Y., P. A. Smith, and J. W. King (1983), A new solar index which leads to improved foF2 predictions using the CCIR Atlas, *Telecomm. J., 50*, p 408.

Liu, L., M. He, X. Yue, B. Ning, and W. Wan (2010), Ionosphere around equinoxes during low solar activity, *J. Geophys. Res., 115*, A09307, doi:10.1029/2010JA015318.

Liu, L., Y. Chen, H. Le, V. I. Kurkin, N. M. Polekh, and C.-C. Lee (2011), The ionosphere under extremely prolonged low solar activity, *J. Geophys. Res., 116*, A04320, doi:10.1029/2010JA016296.

Lühr, H., and C. Xiong (2010), IRI-2007 model overestimates electron density during the 23/24 solar minimum, *Geophys. Res. Lett., 37,* L23010, doi:10.1029/2010GL045430.

Minnis, C., and G. Bazzard (1960), A monthly ionospheric index of solar activity based on F2-layer ionisation at eleven stations, *J. Atmos. Terr. Phys., 18*, p 297-305, doi:10.1016/002191696091136.

Pfaff, R., D. Rowland, H. Freudenreich, K. Bromund, G. Le, M. Acuña, J. Klenzing, C. Liebrecht, S. Martin, W. J. Burke, N. C. Maynard, D. E. Hunton, P. A. Roddy, J. O. Ballenthin, and G. R. Wilson (2010), Observations of DC Electric Fields in the Low Latitude Ionosphere and Their Variations with Local Time, Longitude, and Plasma Density during Extreme Solar Minimum, *J. Geophys. Res., 115,* A12324, doi:10.1029/2010JA016023.

Ren, Z., W. Wan, L. Liu, Y. Chen, and H. Le (2011), Equinoctial asymmetry of ionospheric vertical plasma drifts and its effect on F-region plasma density, *J. Geophys. Res., 116*, A02308, doi:10.1029/2010JA016081.

Rishbeth, H., and O. K. Garriott (1969), “Introduction to ionospheric physics,” Academic Press, New York, NY.

Russell, C. T., J. G. Luhmann, and L. K. Jian (2010), How unprecedented a solar minimum?, *Rev. Geophys., 48*, RG2004, doi:10.1029/2009RG000316.

Savitzky, A., and M. J. E. Golay (1964), Smoothing and differentiation of data by simplified least squares procedures, *Anal. Chem., 36*, p1627.

Scherliess, L. and B. G. Fejer (1999), Radar and satellite global equatorial F region vertical drift model, *J. Geophys. Res., 104*, p 6829-6842.

Schrivjer, C. J., W. C. Livingston, T. N. Woods, and R. A. Mewaldt (2011), The minimal solar activity in 2008-2009 and its implications for long-term climate modeling, *Geophys. Res. Lett., 38,* L06701, doi:10.1029/2011GL046658.

Sibanda, P., and L. A. McKinnell (2011), Topside ionospheric vertical electron density profile reconstruction using GPS and ionosonde data: possibilities for South Africa, *Ann. Geophys., 29*, 229236, doi:10.5194/angeo-29-229-2011

Solomon, S. C., T. N. Woods, L. V. Didkovsky, J. T. Emmert, and L. Qian (2010), Anomalously low solar extreme-ultraviolet irradiance and thermospheric density during solar minimum, *Geophys. Res. Lett., 37,* L16103, doi:10.1029/2010GL044468.

Solomon, S. C., L. Qian, L. V. Didkovsky, R. A. Viereck, and T. N. Woods (2011), Causes of low thermospheric density during the 2007-2009 solar minimum, *J. Geophys. Res., 116*, A00H07, doi:10.1029/2011JA016508.

West, K. H., R. A. Heelis, and F. J. Rich (1997), Solar activity variations in the composition of the low latitude ionosphere, *J. Geophys. Res., 102*, 295305, doi:10.1029/96JA03031.

Table 1. Seasonal divisions for the topside profile reconstructions, including the average solar activity represented by F10.7, Rz_{12}, and IG_{12} for each period.

Period	Range of Days	F10.7	Rz_{12}	IG_{12}
Sep Equinox 2008	8 Aug 2008 – 6 Nov 2008	67.8	2.3	-10.1
Dec Solstice 2008	6 Nov 2008 – 4 Feb 2009	67.3	2.0	-9.2
Mar Equinox 2009	3 Feb 2009 – 4 May 2009	69.2	2.0	-8.4
Jun Solstice 2009	7 May 2009 – 5 Aug 2009	70.9	3.2	-6.3
Sep Equinox 2009	8 Aug 2009 – 6 Nov 2009	70.9	6.2	-0.8
Dec Solstice 2009	6 Nov 2009 – 4 Feb 2010	75.5	8.5	3.9
Mar Equinox 2010	3 Feb 2010 – 4 May 2010	80.3	12.5	10.3
Jun Solstice 2010	7 May 2010 – 5 Aug 2010	77.9	16.8	15.7
Sep Equinox 2010	8 Aug 2010 – 6 Nov 2010	81.5	21.0	19.0
Dec Solstice 2010	6 Nov 2010 – 31 Jan 2011	81.6	29.1	26.2

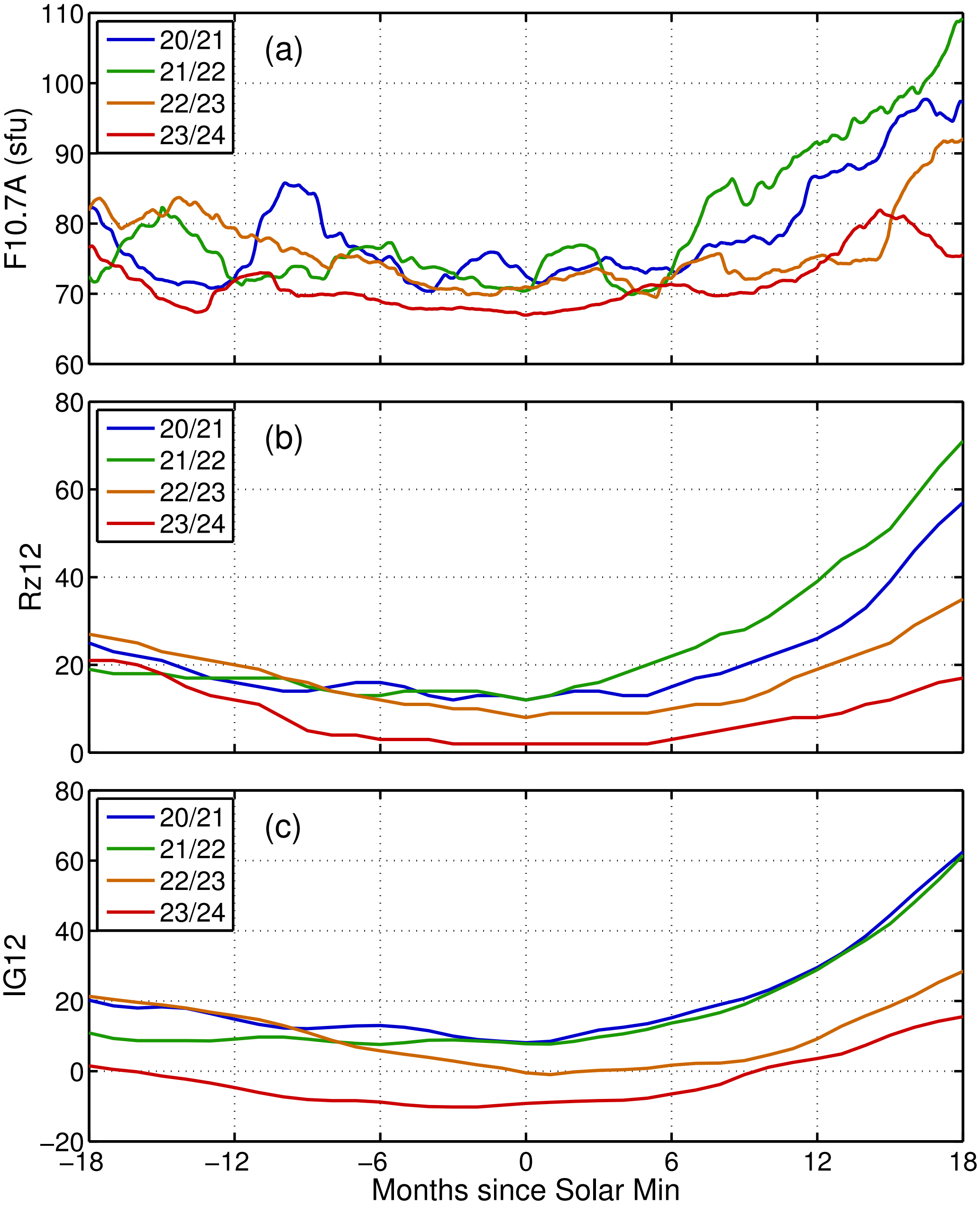

Figure 1. Solar activity near the solar minima for the last three cycles, inlcuding (a) F10.7A, (b) Rz_{12}, and (c) IG_{12}. The F10.7A values are 81-day averages, and the Rz_{12} and IG_{12} indices are 12-month averages. Rz_{12} and IG_{12} are used to drive the IRI-2007 model in this study.

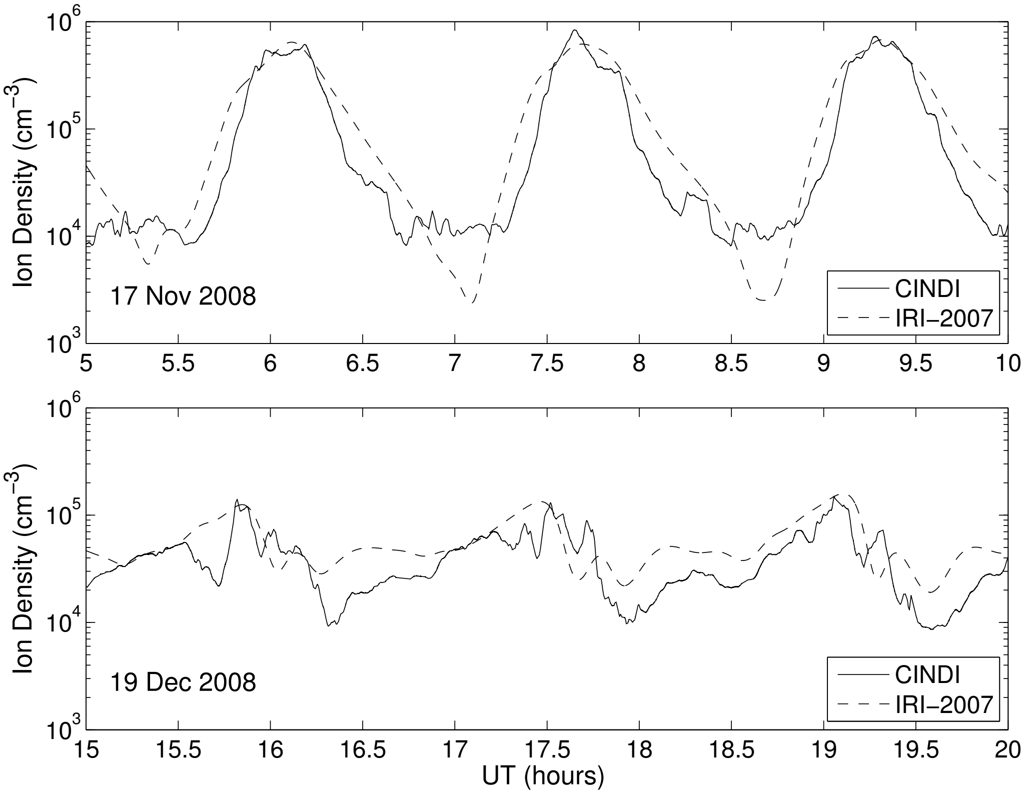

Figure 2. The variability of C/NOFS density data, along with the expected values based on IRI-2007. The top panel shows five hours (roughly three orbits) from 17 Nov 2008 (when perigee is at local noon), and the bottom panel shows the same for 19 Dec 2008 (when perigee is at local midnight)

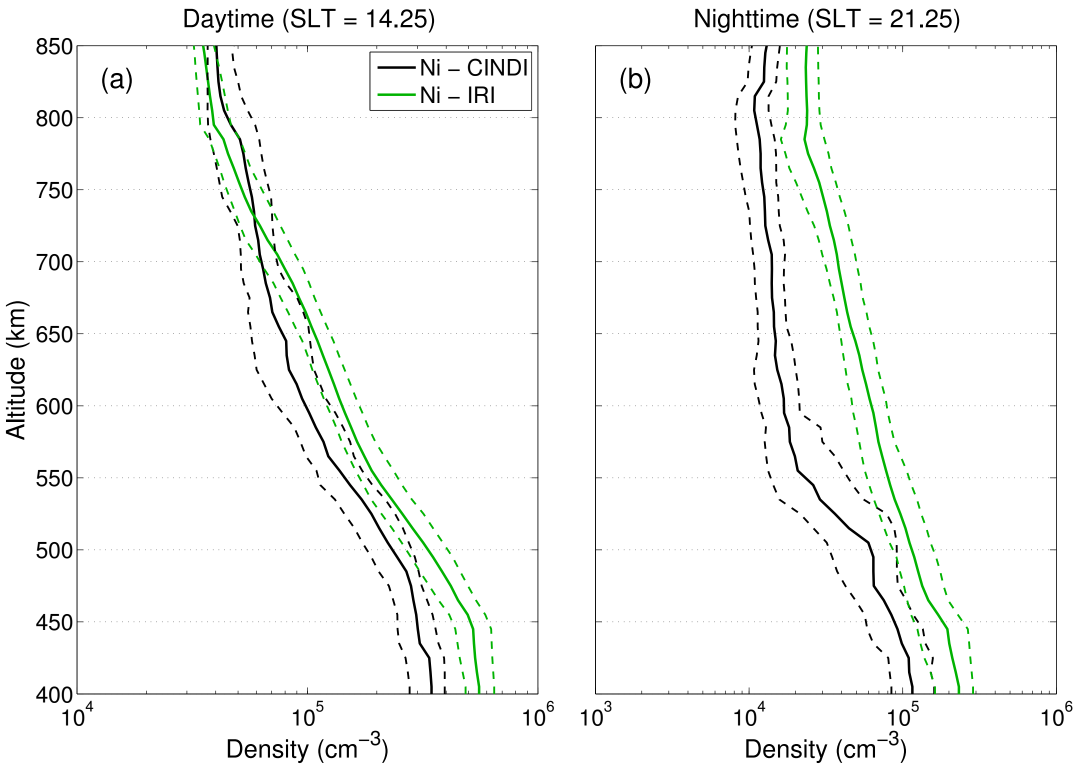

Figure 3. A sample reconstructed altitude profile based on the average C/NOFS CINDI data (black) for the topside equatorial ionosphere for the December solstice of 2008, along with the associated IRI-2007 profile (green). The solid lines represent the median density profile; the dashed lines represent the first and third quartiles. The left panel is a dayside profile, centered around 14.25 local time; and the right panel is a nightside profile, centered around 21.25 local time.

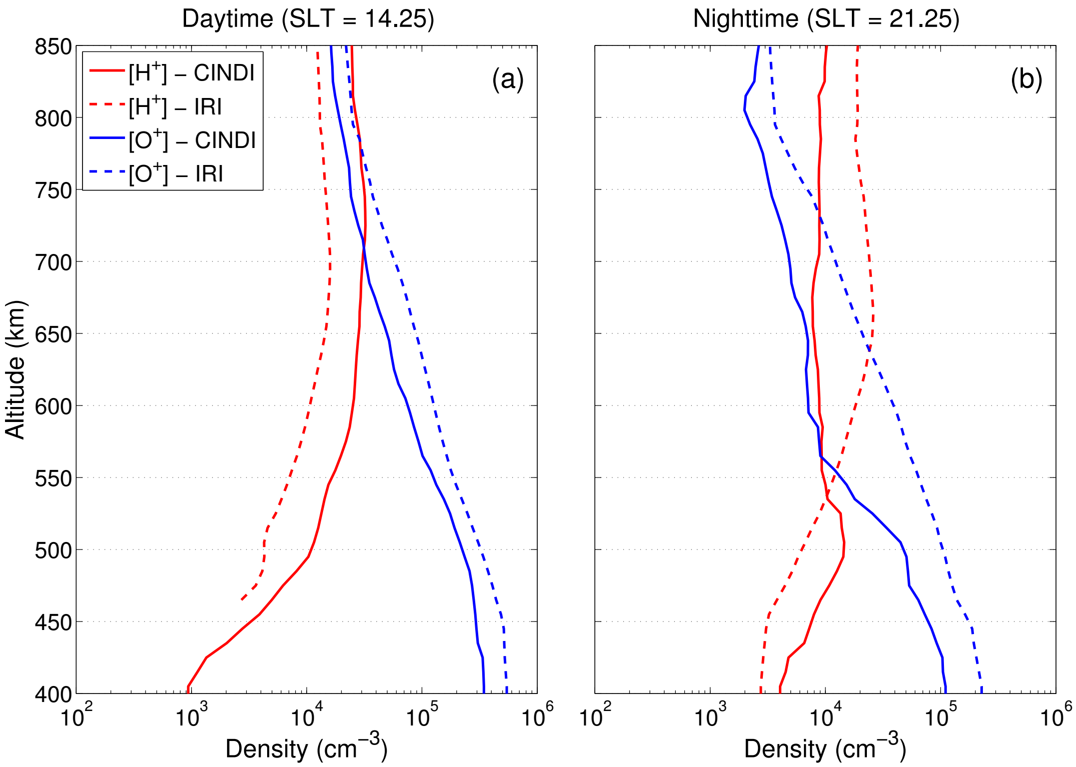

Figure 4. The composition profiles associated with the density profiles from Figure 3. The two major component ions are H^+ (red) and O^+ (blue). Note that while the total ion density matched IRI quite well for the dayside profiles, the composition is quite different. For both dayside and nightside, the transition height between H^+ and O^+ is lower than predicted.

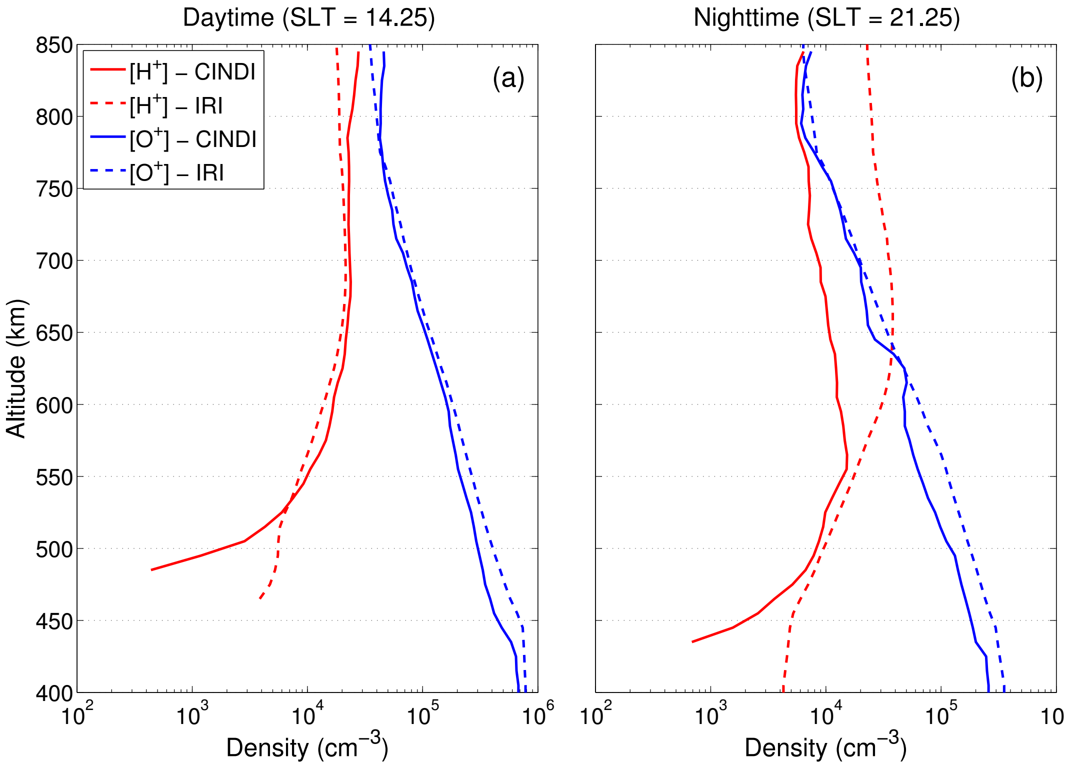

Figure 5. The same as Figure 4, but for the December solstice of 2010 (2 years later). Note that the nightside transition height between O^+ and H^+ is now very similar for both the measurements and the model.

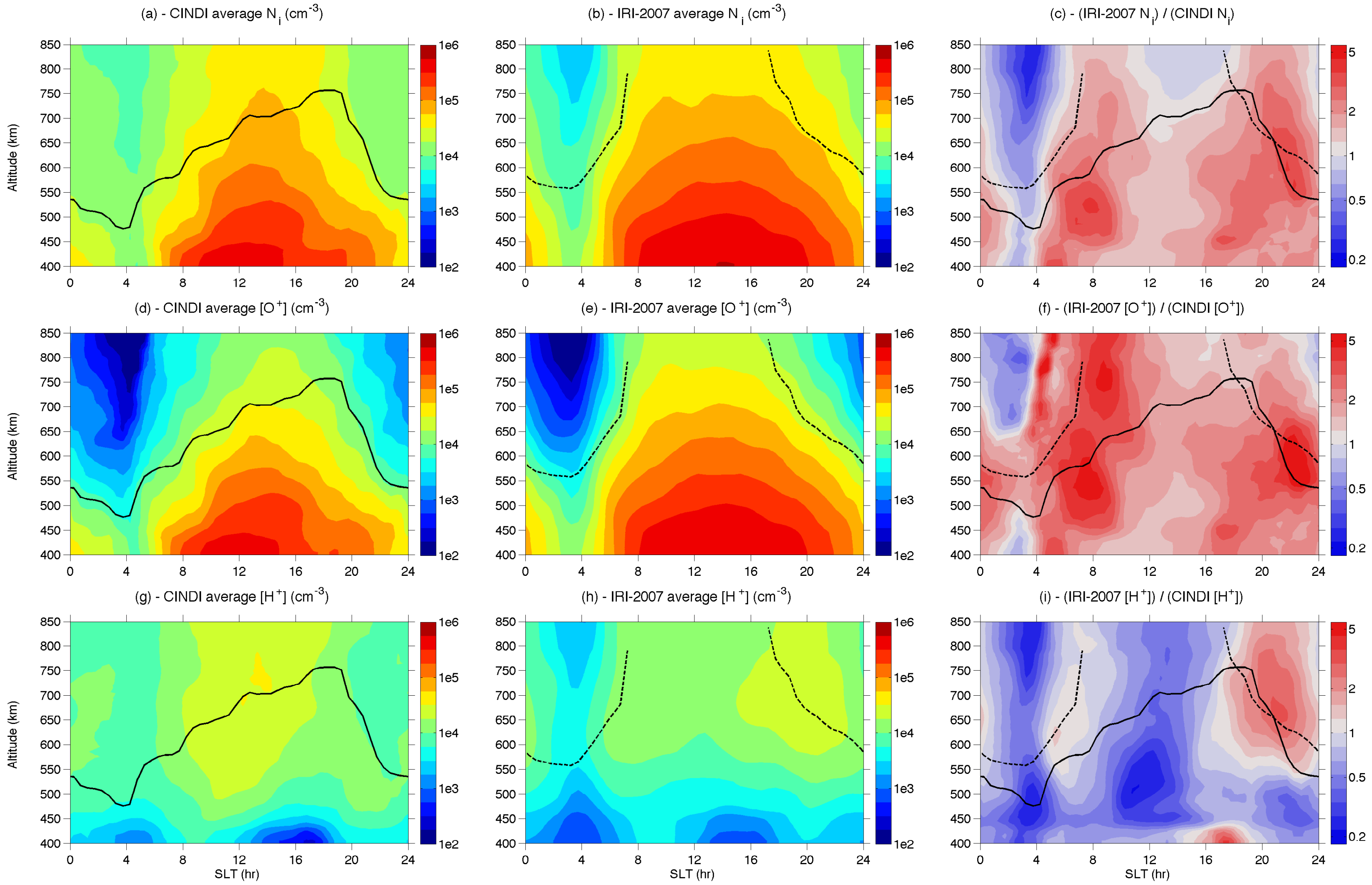

Figure 6. The average total and component densities as a function of altitude and local time for the December solstice 2008. Panel (a) shows the average total ion density, while panel (b) shows the average expected densities based on IRI-2007. Panel (c) is the ratio of the expected density to the measured values. The other rows show the same for the O$^+$ component (d-f) and the H$^+$ component (g-i).

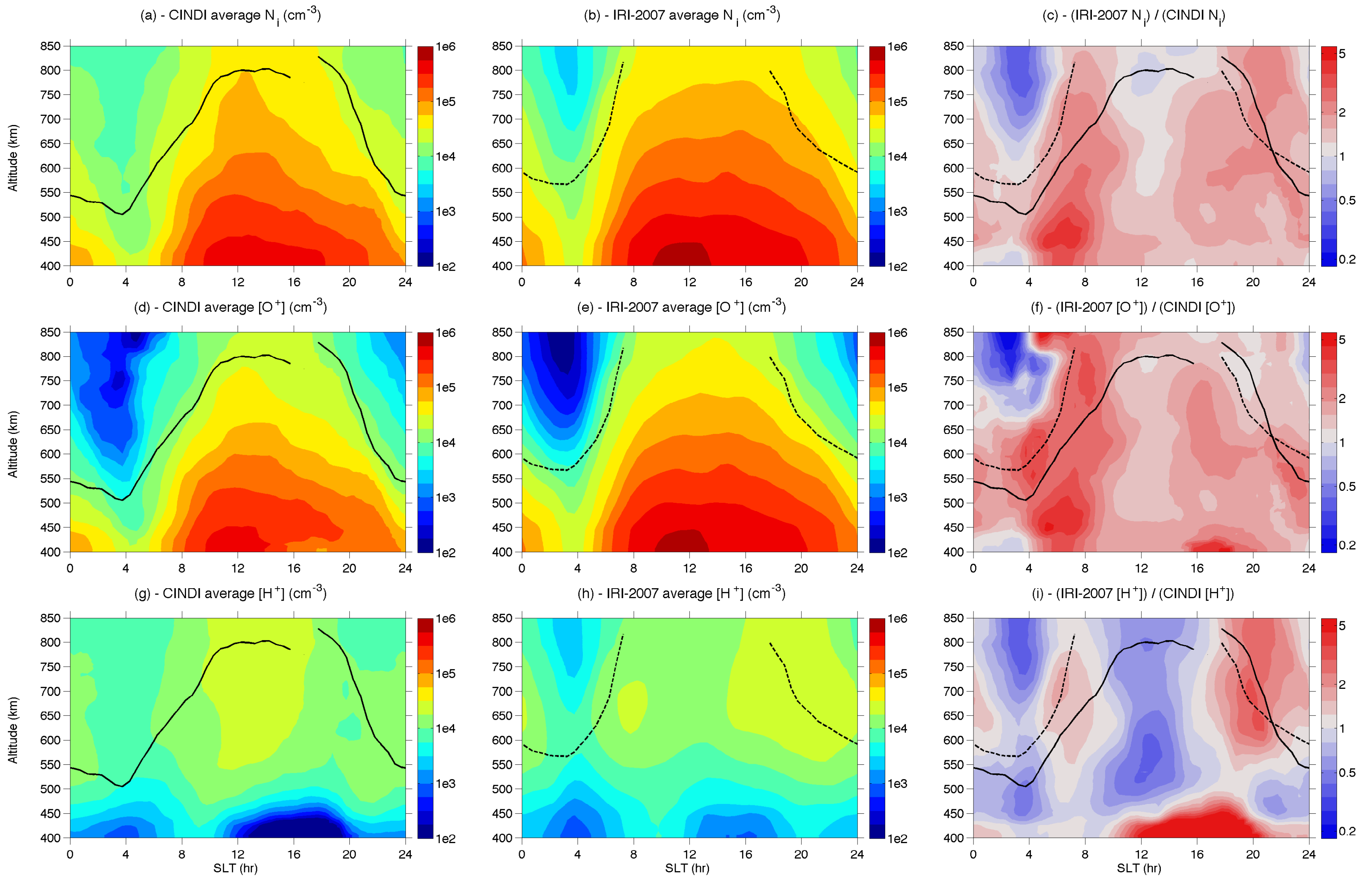

Figure 7. The average total and component densities as a function of altitude and local time for the December solstice 2009. The format is the same as in Figure 6.

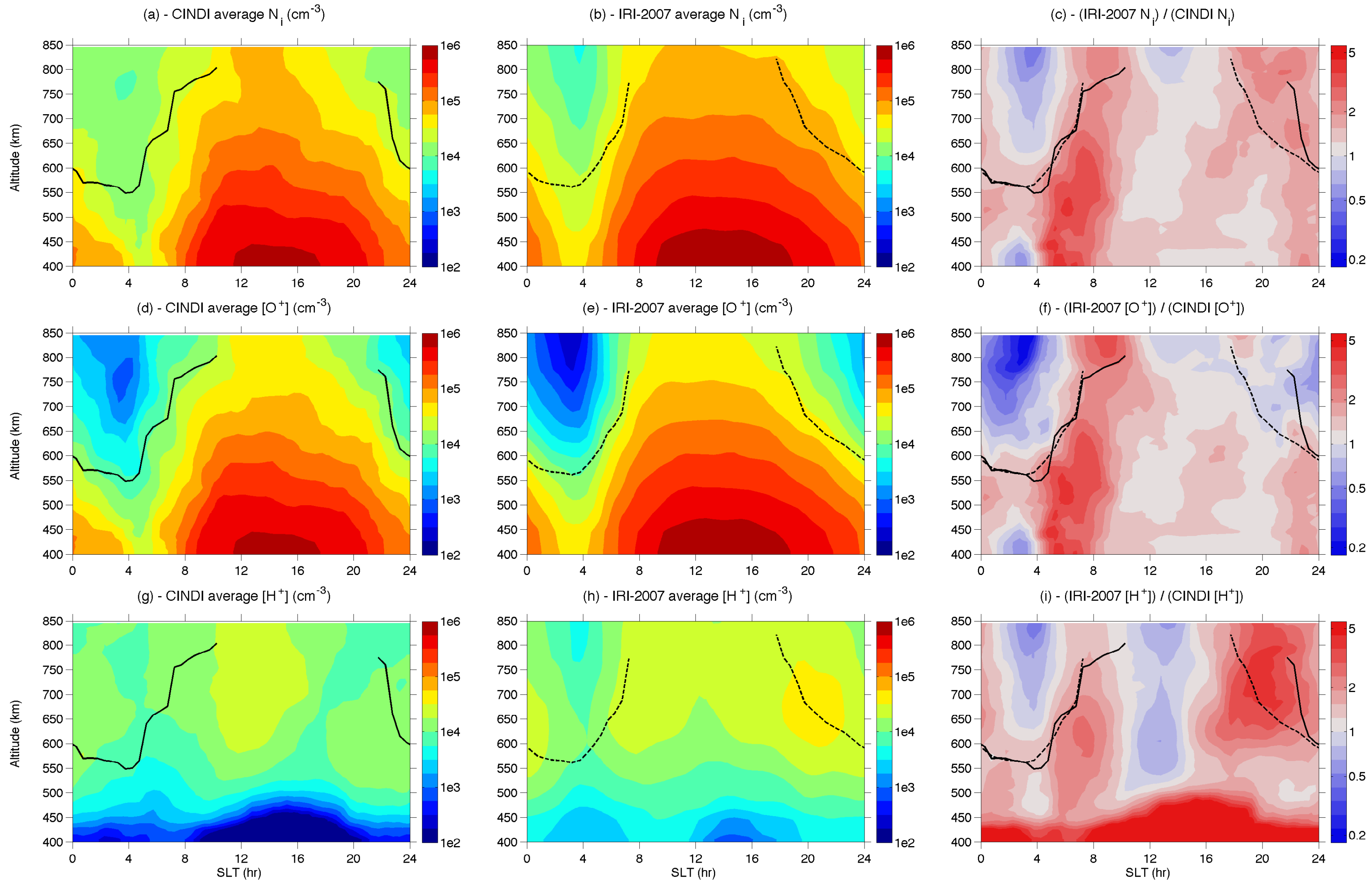

Figure 8. The average total and component densities as a function of altitude and local time for the December solstice 2010. The format is the same as in Figure 6.

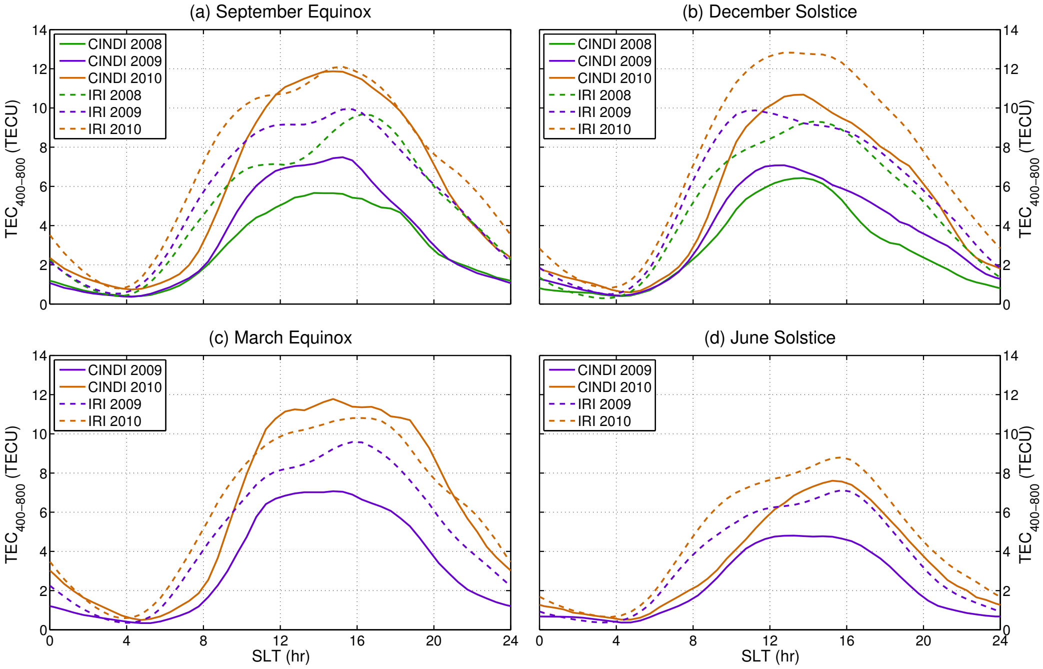

Figure 9. The "total" electron content between 400 and 800 km as a function of solar local time. These plots capture the seasonal and temporal variation of density for (a) September equinox, (b) December solstice, (c) March equinox, and (d) June solstice. Note that the measured densities are significantly lower than predicted by IRI until the March equinox of 2010.

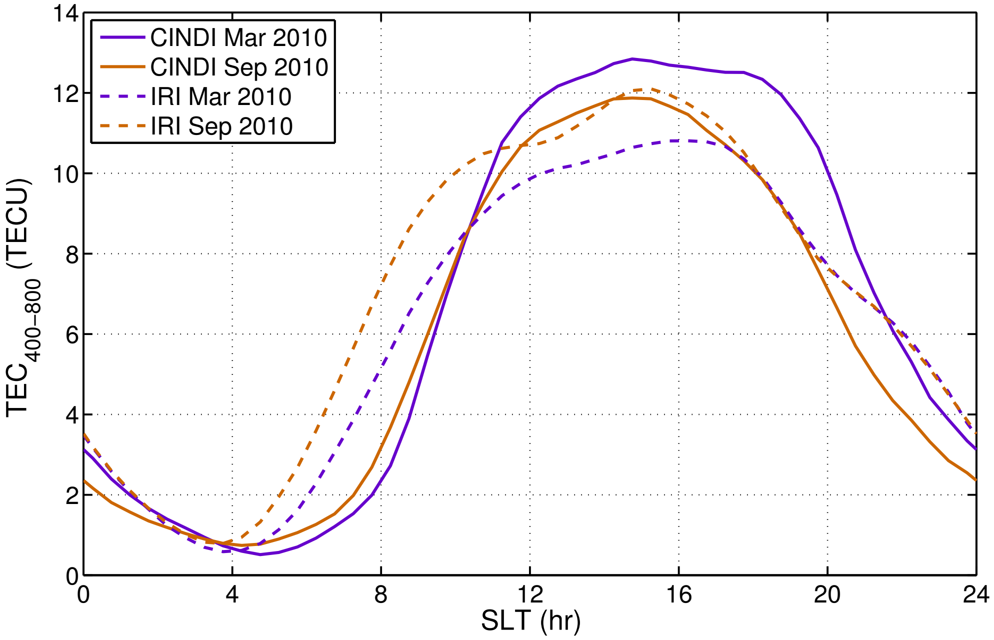

Figure 10. Selected data from Figure 9 replotted to illustrate the equinoctial asymmetry during 2010. The March equinox TEC is larger than the corresponding data in the September Equinox after ∼10.5 SLT.

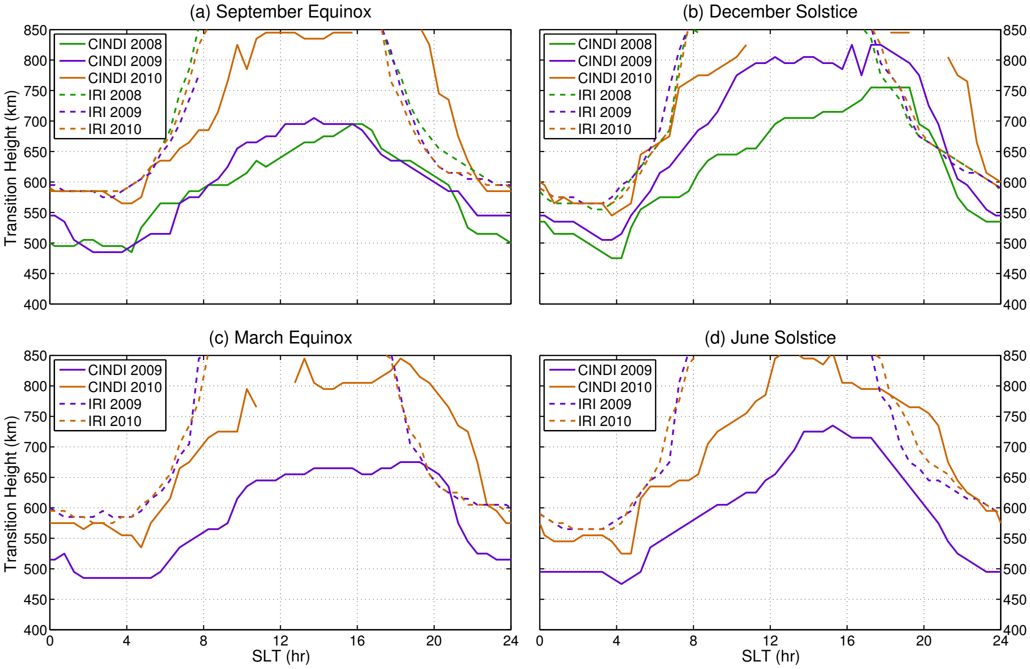

Figure 11. The transition height between H^+ and O^+ as a function of solar local time. These plots capture the seasonal and temporal variation for (a) September equinox, (b) December solstice, (c) March equinox, and (d) June solstice. Note that the daytime transition height as predicted by IRI is above the range of the C/NOFS satellite.

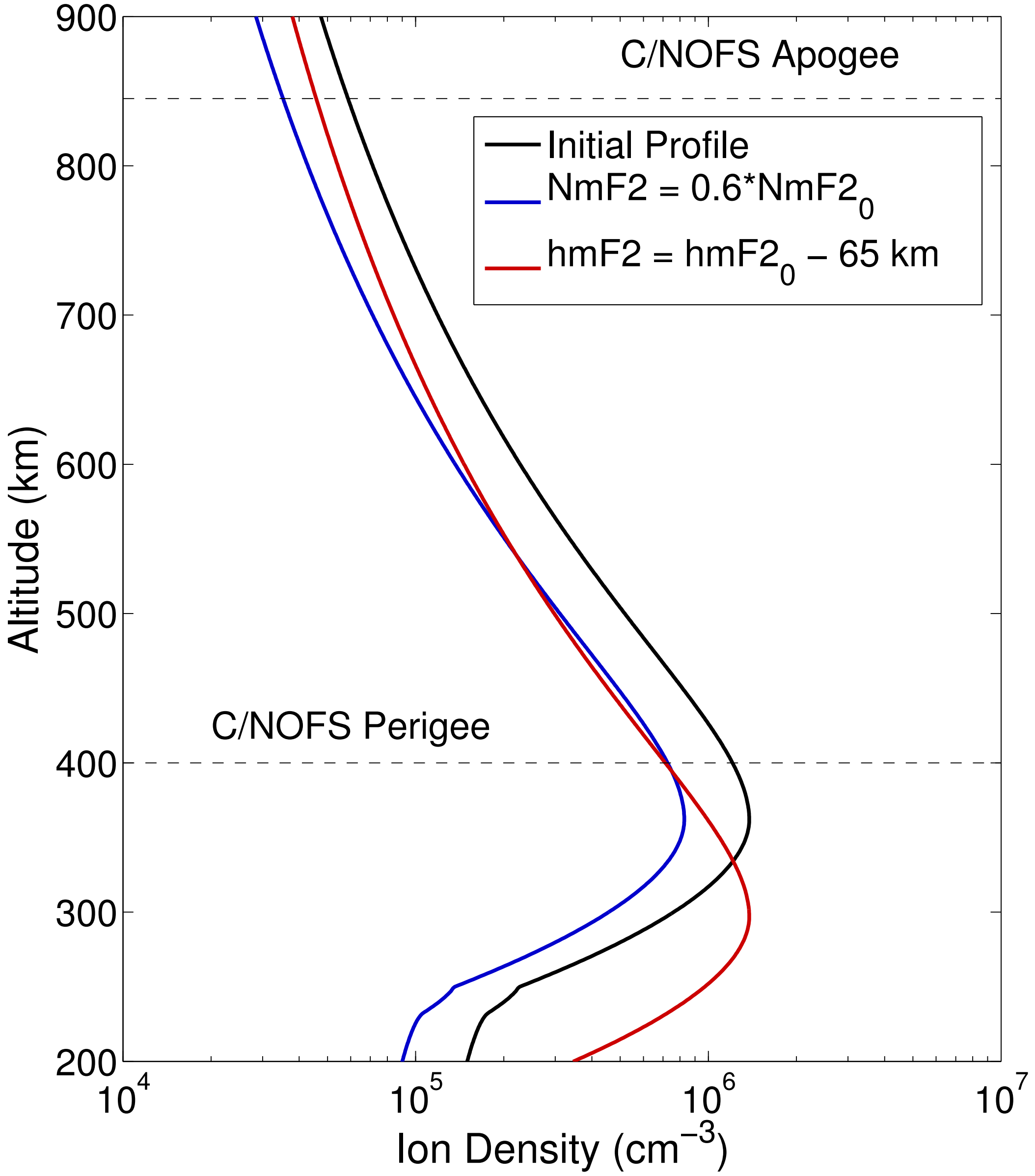

Figure 12. The effects of changing the position of the $F-$peak on the observed topside profile. An initial profile (black) is generated using IRI-2007. Two altered profiles are included: one where NmF2 is scaled down by 60% (blue), and one where hmF2 is moved down by 65 km. The apogee and perigee of the C/NOFS satellite are shown as dashed lines.